This is a preprint, the final version is subject to change, of the American Mineralogist (MSA)
Cite as Authors (Year) Title. American Mineralogist, in press.
DOI: https://doi.org/10.2138/am-2020-7456

REVISION 1

Magmatic haggertyite in olivine lamproites of the West Kimberley region, Western Australia

A. Lynton Jaques[1*], Frank Brink[2] and Jiang Chen[2]

1. Research School of Earth Sciences, Australian National University, 142 Mills Road, Canberra, ACT 2601, Australia.

2. Centre for Advanced Microscopy, Australian National University, 131 Garran Road, Canberra, ACT 2601, Australia

* E-mail: lynton.jaques@anu.edu.au

This is a preprint, the final version is subject to change, of the American Mineralogist (MSA)
Cite as Authors (Year) Title. American Mineralogist, in press.
DOI: https://doi.org/10.2138/am-2020-7456

ABSTRACT

We report the first occurrence of magmatic haggertyite ($BaFe_6Ti_5MgO_{19}$) from the Miocene lamproites of the West Kimberley region of Western Australia. This contrasts with the metasomatic formation reported in an olivine lamproite host at the type locality, Prairie Creek, Arkansas. Haggertyite occurs in the groundmass of a diamondiferous olivine lamproite pipe in the Ellendale field, and within the large zoned Walgidee Hills lamproite where it forms part of an extensive suite of Ba- and K- bearing titanate and Ti-rich silicate minerals. The haggertyite coexists with chromian spinel, perovskite and ilmenite in the Ellendale lamproite, and with priderite and perovskite and, in one locality, with priderite, jeppeite, ilmenite and perovskite, in the Walgidee Hills lamproite. Unlike priderite and perovskite which are common groundmass phases in the Ellendale olivine lamproites and present throughout the Walgidee Hills lamproite, haggertyite appears restricted in its occurrence and crystallization interval, with sparse ilmenite apparently mostly crystallizing as an alternative phase. In the Walgidee Hills lamproite the haggertyite-bearing assemblage is succeeded by the Ba-titanate assemblage priderite plus jeppeite in the evolved central part of the body.

The haggertyite in the main zone of the Walgidee Hills lamproite has an average composition of $(Ba_{0.7}K_{0.3})_{1.0}[Ti_{5.0}Fe^{3+}_{2.1}Cr_{0.1}Fe^{2+}_{3.8}Mn_{0.2}Mg_{0.6}Na_{0.1}]_{12}O_{19}$ and is thus very similar to the original haggertyite described from xenoliths in the Prairie Creek lamproite apart from being poorer in Cr and Ni. Haggertyite in the groundmass of the Ellendale olivine lamproite and the central zone of the Walgidee Hills lamproite, in addition to variations in Mg and Cr, show significant variation in Ti and Fe contents and in calculated Fe^{3+} and Fe^{2+}. A linear inverse relationship between Ti and Fe, and Ti and Fe^{3+}, indicates that Fe^{3+} is accommodated by the coupled substitution $Ti^{4+} + Fe^{2+} \leftrightarrows 2\ Fe^{3+}$. A marked trend to higher Fe^{3+} in the haggertyite in Ellendale 9 olivine lamproite is ascribed to increasing oxidation during crystallization, with fO_2 estimated from the olivine-spinel thermometer and oxygen barometer at Δlog FMQ = -1 to +3 at temperatures of 790−660 °C. The haggertyite in the central zone of the Walgidee Hills lamproite, in contrast, shows a marked trend to Fe^{2+}

enrichment which is associated with decreasing Fe in perovskite. This is inferred to indicate formation under more reducing conditions, but sufficiently oxidized to permit Fe^{3+} in coexisting priderite and jeppeite.

Trace element analysis by LA-ICP-MS shows the Walgidee Hills haggertyite contains minor amounts of Na, Si, Ca, V, Co, Zn, Sr, Zr, Nb, and Pb, and only traces of Al, P, Sc, Rb, REE, Hf and Ta. Moreover, the haggertyite is preferentially enriched in certain lithophile (Ba, Sr), siderophile (Mn, Fe, Co, Ni) and chalcophile (Zn, Pb) elements relative to co-existing priderite. Haggertyite crystallization appears to be a consequence not only of the very high Ba, Ti, and K contents of the lamproite, but of relatively high Fe concentrations and low temperatures in evolved olivine lamproite magma with the Fe^{3+}/Fe^{2+} ratio determined by the prevailing fO_2. The new data suggest that haggertyite might also be present but previously unrecognized in the evolved groundmass of other olivine lamproites. Haggertyite is one of an increasing number of new minerals in upper mantle rocks and volcanics derived from the upper mantle hosting large-ion-lithophile and high field strength cations.

Keywords: haggertyite, titanate, ultrapotassic, lamproite, priderite, magneto-plumbite, ilmenite.

INTRODUCTION

Haggertyite is a rare magnetoplumbite-structured K-Ba titanate with the general formula $Ba[Fe_6Ti_5Mg]O_{19}$ named in honour of Professor Stephen Haggerty (Grey et al. 1998). It was first described from the Prairie Creek lamproite, Arkansas, USA (Mitchell and Bergman 1991 and references therein) where it occurs exclusively in a narrow reaction zone between the olivine lamproite host and serpentinized xenoliths (Grey et al. 1998; Velde 2000). Velde (2000) interpreted the xenoliths to represent quenched ultramafic magma (possibly komatiite) and proposed that the haggertyite formed as a result of chemical diffusion between the highly contrasting compositions of the xenolith and the ultrapotassic lamproite host.

This paper reports a second occurrence of haggertyite, this time as a magmatic phase. The haggertyite occurs as part of the crystallization sequence in olivine lamproites of the Miocene West Kimberley lamproite province in northern Western Australia (Jaques et al. 1984a, 1986). We describe haggertyite from two separate lamproite bodies. In the large zoned Walgidee Hills lamproite, haggertyite coexists with other titanates over a short crystallisation interval in several localities within the main zone of the intrusion and, in one locality, within the central zone of the body. Haggertyite was also found in the groundmass of a potassium richterite–phlogopite–olivine lamproite from near the centre of the Ellendale 9 olivine lamproite.

Modally small concentrations of minerals hosting high field strength (HFS) and large-ion-lithophile (LIL) elements may be important hosts of such elements in metasomatized and chemically enriched sub-continental lithospheric mantle (e.g. Haggerty 1989, 1995). A wide variety of potassic alkaline rocks, including lamproites, are generally thought to be derived by small degrees of partial melting of such enriched lithospheric mantle (e.g. Mitchell and Bergman 1991; Mitchell 1995; Tappe et al. 2013; Giuliani et al. 2015; Jaques et al. 2018). The extreme enrichment in LIL and HFS elements in these mantle-derived magmas results, in turn, in crystallization of a complex array of alkali titanate minerals.

GEOLOGICAL SETTING

The Walgidee Hills lamproite in Western Australia (Fig. 1) forms part of the Miocene West Kimberley lamproite province which lies at the southwest margin of the Kimberley Craton extending from the Proterozoic King Leopold Orogen bordering the craton across the Fitzroy Trough in the northern Canning Basin. The province comprises some 180 individual bodies which occur as volcanic pipes, plugs, sills and dykes clustered in three main fields (Jaques et al. 1984a, 1986). The Ellendale field in the north consists mostly of olivine-rich lamproite pipes and isolated leucite lamproite volcanic plugs and sills, whereas the Noonkanbah field in the south is dominated by leucite-rich lamproite plugs, sills and dykes (Wade and Prider 1940; Prider 1965; Jaques et al. 1984a, 1986).

The Walgidee Hills lamproite is the largest (~2.5 km in diameter) and, at 17.5 Ma, the youngest lamproite in the West Kimberley lamproite province which range in ages from ~21 to 17.5 Ma (Jaques et al. 1984b, 1986; Phillips et al. 2013). Waldigee Hills is the site of original descriptions of several K-, Ba- and Ti-rich minerals characteristic of lamproites, including priderite [$(K,Ba)(Ti,Fe^{3+})_8O_{16}$], wadeite ($K_2ZrSi_3O_9$), jeppeite [$(K,Ba)_2(Ti,Fe)_6O_{13}$], and noonkanbahite ($BaKNaTi_2Si_4O_{14}$: Prider 1939, 1965; Wade and Prider 1940; Norrish 1951; Pryce et al. 1984; Jaques 2016). Geological mapping and company exploration drilling (e.g. Drury 1998; Ceplecha, 2000 and earlier references therein) have shown the Walgidee Hills lamproite to be a pipe-like intrusion concentrically zoned in terms of grain size, mineralogy, and rock composition (Jaques, 2017). Rock types range from porphyritic olivine (altered) lamproite at the margin of the intrusion through medium-grained lamproite comprised of olivine (altered) xenocrysts and phenocrysts in a matrix of diopside, titanian phlogopite (Ti-phlogopite), leucite (altered but with very rare surviving included crystals), and titanian potassium richterite (Ti-K-richterite) to coarse grained and pegmatitic Ti-phlogopite−diopside−Ti-K-richterite–sanidine lamproite at the centre (Fig. 1). Priderite, perovskite, apatite, and wadeite are constant accessory minerals throughout the body, ilmenite occurs sporadically, and jeppeite and noonkanbahite occur only at the centre of the intrusion (Jaques et al. 1986, Jaques 2017). A pronounced coarsening in grain size of the lamproite toward the centre of the intrusion is accompanied by a decrease in MgO, Ni and Cr contents, and an increase in Fe, Ti, Y, Zr, Nb, Hf, Rb, REE, and Th abundances inwards to the most evolved rocks at the centre of intrusion. Lithological

zoning from the margins to the centre of the intrusion and textural relationships within samples suggests that the paragenetic sequence is: olivine – chromian spinel – diopside − perovskite – leucite – phlogopite – apatite – wadeite – priderite – (haggertyite or ilmenite) – titanian potassium richterite – sanidine – jeppeite – noonkanbahite (Jaques 2017). The distribution of haggertyite appears to be limited and apparently confined to a relatively few locations near the centre of lamproite (Fig. 1).

The Ellendale 9 lamproite (47 ha) is a complex volcanic pipe comprised of basal tuffs formed by multiple eruptions and overlain by olivine lamproite interpreted to be a former lava lake infilling the pipe (Jaques et al. 1986; Stachel et al. 1994). Ellendale 9 carries diamonds at low concentrations and, together with the nearby Ellendale 4 pipe, was mined in the period 2002−2015 producing more than 2.1 million carats (Ahmat 2012). The sample containing haggertyite comes from near the centre of the coarser grained central part of the pipe, and is comprised of olivine xenocrysts and macrocrysts up to 2.5 cm across together with smaller olivine phenocrysts (<1 mm) set in a crystalline groundmass of abundant poikilitic plates of phlogopite (up to 1 mm) and interstitial Ti-K-richterite (up to 200 μm) containing inclusions of diopside, chrome spinel, perovskite, wadeite, ilmenite, and altered former leucite (Jaques et al. 1986; Stachel et al. 1994). Detailed accounts of the geology (including maps and sections), petrography, mineralogy and geochemistry of the Ellendale 9 pipe are given elsewhere (Jaques et al. 1986; Stachel et al. 1994; Jaques 2016; Jaques and Foley 2018).

METHODS

Electron probe analyses and back-scattered electron images

Most of the analyses and many of the back-scattered electron (BSE) images presented here were obtained using a JEOL 8530F Plus electron probe micro-analyser (EPMA) equipped with 5 wavelength-dispersive spectrometers and a Schottky Field Emission (FE) gun at the Centre for Advanced Microscopy (CAM) at the Australian National University (ANU). Analyses were made at 15 kV and 30 or 50 nA using a spot size of 2 μm. Counting times were 20 seconds (peak and background) for major elements and 30−40 seconds for minor

elements. Calibrations were made using a mix of synthetic and natural ASTIMEX mineral and metal standards as follows: Na (albite), Mg (MgO), Al (sanidine), Si (diopside), Ca (diopside), Ti (rutile), V (vanadium metal), Cr (Cr_2O_3), Mn (rhodonite), Fe (haematite), Ni (pentlandite), Zn (willemite), and Ba (barite). Iron metal and ASTIMEX and USNM (Jarosewich et al. 1980) standards including benitoite, chromite, and magnetite were used as secondary standards to monitor the analysis quality. Limits of detection were typically 70−180 ppm, except for Zn and Ba (~250 ppm), equivalent to 0.01−0.03 wt% oxide. Data were reduced using the 'PAP model' corrections (Pouchou and Pichoir 1991). A small number of analyses were initially made using a Cameca SX-100 EPMA at the Research School of Earth Sciences (RSES) at the ANU equipped with 4 wavelength-dispersive spectrometers during a study of the groundmass phases of the West Kimberley lamproites (Jaques 2016). Analyses were acquired at 15 kV using a 2-condition routine in which Na, Mg, Al, Si, K, Ca, Ti, Cr, Mn and Fe were determined with a beam current of 20 nA and beam size of ~1 μm and counting times of 40–120 seconds (peak and backgrounds). Limits of detection were typically 0.02–0.04 wt% oxide. Barium, V, Sr, Zr, and Nb were determined using a beam current of 100 nA with longer counting times but similar limits of detection (Jaques 2016). Sr, Zr and Nb concentrations in the haggertyite were mostly at or below detection limits. Agreement between the two sets of EPMA analyses was excellent (≤1% relative for the average K, Ti, Fe and Ba compositions).

BSE images and quantitative energy-dispersive X-ray spectrometer (EDS) analyses for one sample were obtained using a Hitachi 4300 SE/N SEM equipped with a Schottky Field Emission gun and Oxford Instruments INCA X-Max EDS analytical system at CAM, ANU. Analyses were made at 15 kV and 0.6 nA with calibrations made using the same standards as the JEOL 8530F Plus EPMA. Agreement between EPMA WDS and SEM quantitative EDS data was excellent for the major elements Mg, K, Ti, Cr, Mn, Fe and Ba.

Additional images were obtained using a JEOL JSM-6610A SEM fitted with JEOL BSE and EDS detector at the RSES, and a FEI Quanta QEMSCAN® Field Emission SEM equipped with twin EDS detectors at CAM.

Both instruments operated at 15 kV with images obtained at ~10 and ~3 nA with working distances of 11 and 13 mm respectively.

Trace element analyses

The trace elements – ^{23}Na, ^{24}Mg, ^{27}Al, ^{29}Si, ^{31}P, ^{39}K, ^{43}Ca, ^{45}Sc, ^{49}Ti, ^{51}V, ^{53}Cr,^{55}Mn, ^{57}Fe, ^{59}Co, ^{60}Ni, ^{63}Cu, ^{66}Zn, ^{69}Ga, ^{85}Rb, ^{88}Sr, ^{89}Y, ^{90}Zr, ^{93}Nb, ^{137}Ba, ^{139}La, ^{140}Ce, ^{141}Pr, ^{146}Nd, ^{147}Sm, ^{153}Eu, ^{157}Gd, ^{163}Dy, ^{166}Er, ^{172}Yb, ^{178}Hf, ^{181}Ta, ^{208}Pb, ^{232}Th and ^{238}U − were determined by laser-ablation inductively-coupled-plasma mass-spectrometry (LA-ICP-MS) at RSES using an Agilent Technologies 7700 ICP-MS coupled to an ANU HelEX laser-ablation system with a 193 nm wavelength EXCIMER laser (110 (ArF) COMPex, Lambda Physik) following the method of Eggins et al. (1997) and Jenner and O'Neill (2012). Data acquisition involved a 20 second background measurement followed by 45 seconds of ablation, 5 Hz repetition rate and a fluence of ~5 J/cm^2 (Jaques 2016). The laser spot size was mostly 60 μm with a smaller number analysed with a 20 μm spot. Mineral unknowns were analysed by bracketing every 5−10 unknowns with analyses of NIST reference glasses SRM 610 and 612 (Jochum et al. 2011) and BCR-2G (GeoRem, Jochum et al. 2005). Titanium compositions determined by EPMA were used as an internal standard and NIST SRM 610 was used as the reference standard. BCR-2G and NIST SRM 612 were measured as unknowns and monitored for data quality control. Data were processed using the Iolite v2.5 software package (Paton et al. 2011). The measured concentrations for all elements except Sc and Zn (17% and 37% higher than the reference values respectively) are within 15% of the reference value for BCR-2G (GeoREM: Jochum et al. 2005, 2011), with more than three quarters of the elements analyzed lying with ± 5% of the reference value. The analysis of REE and other trace elements at low concentrations (≤1 ppm) in haggertyite proved problematic as previously found for priderite and jeppeite and these analyses have a large uncertainty (Jaques 2016).

PETROGRAPHY OF THE HAGGERTYITE AND ASSOCIATED MINERALS

Walgidee Hills

The haggertyite was first noted as sparse grains of an unidentified K-Ba-Fe titanate (Jaques unpub. data; Miller 1996) in polished thin sections of several medium grained lamproites of the Walgidee Hills lamproite (Fig. 1). Subsequent EPMA analyses by WDS confirmed the mineral was haggertyite and further examination found additional samples with haggertyite. The haggertyite varies in size and shape, and in its associated titanate phases.

Most of the haggertyite occurs as sparse grains in medium-grained Ti-phlogopite–diopside–Ti-K-richterite–olivine−leucite lamproite of the main zone that surrounds the coarse-grained to pegmatitic Ti-phlogopite−diopside−Ti-K-richterite–sanidine lamproite at the centre of the Walgidee Hills lamproite. The lamproites in the main zone are petrographically similar, containing sparse altered former olivine xenocrysts up to 5 mm across and smaller (100−500 μm) sub-to euhedral olivine phenocrysts, all of which are altered to serpentine and smectite. These are set in a matrix containing euhedral diopside prisms (typically 200−500 μm but up to ~750 μm), sparse large (1.5−5 mm) plates of Ti-phlogopite, abundant pleochroic interstitial Ti-K-richterite up to ~4 mm with abundant altered former leucite (now altered to secondary potash felspar and smectite) and smaller sub- to euhedral grains of sanidine. Euhedral priderite (up to 1 mm long but more typically 100−500 μm), and smaller euhedra (50–150 μm) of apatite, perovskite, and wadeite are present as conspicuous accessory minerals comprising up to 5 vol% of the rock. The lamproites containing the haggertyite in this part of the intrusion have similar whole rock compositions characterized by high K_2O, TiO_2 and BaO (~4−5 wt% K_2O, TiO_2; 0.7−1.3 wt% BaO), and moderate Fe and high MgO (6−7 wt% total Fe as FeO; 15−18 wt% MgO) contents. In these rocks the haggertyite occurs closely associated with priderite from which it can be distinguished by the absence of the strong pleochroism, twinning, striped or ribbed appearance, and etch pits characteristic of priderite (Fig. 2a−d).

The haggertyite in sample 353 (Fig. 1) occurs as sparse sub-to euhedral grains 50−500 μm co-existing with abundant euhedral priderite mostly 100−500 μm but up to 1 mm long (Fig. 2a−d). The haggertyite occurs as both discrete grains and in mutual contact with the priderite (Fig. 2a−d). Both the haggertyite and priderite are

commonly partially or wholly enclosed in Ti-K richterite which forms large (up to 4 mm) poikilitic plates with pale pink−to−lemon pleochroism. Larger grains of haggertyite, and especially priderite, commonly have inclusions of euhedral earlier crystallized diopside, perovskite, wadeite, and leucite. Compositions of the haggertyite are given in Table 1 and of co-existing perovskite and priderite in Table 2 and Jaques (2016).

In sample 213 (Fig. 1) the haggertyite occurs as small subhedral grains (up to ~200 μm, mostly ≤150 μm) in the matrix of the lamproite, again associated with perovskite and more abundant larger (up to 500 μm) priderite grains. Compositions of the haggertyite are given in Table 1 and the perovskite and priderite are given in Table 2 and Jaques (2016). In sample 185 (Fig. 1) rare small euhedra (<100 μm) of haggertyite are associated with abundant priderite and perovskite, and subordinate ilmenite. Compositions of the haggertyite are given in Supplementary Material and priderite and perovskite are given in Jaques (2016).

Haggertyite was also found in a medium grained diopside–Ti-K-richterite–sanidine lamproite at the margin of the central zone where it co-exists with priderite, perovskite, jeppeite, ilmenite, wadeite, and apatite. The presence of haggertyite, ilmenite and jeppeite in this sample is unusual as elsewhere in the central zone priderite and jeppeite, accompanied by perovskite, are the co-existing titanates. In sample 087 (Fig. 1) rare sub- to euhedral haggertyite grains up to ~250 μm (mostly ≤100 μm) co-exists with common sub- to euhedral priderite (up to 500 μm) and perovskite (up to ~100 μm), and sparse anhedral ilmenite and jeppeite up to 500 μm across (Fig. 3 a−e). Both the haggertyite and other titanates in this sample have resorbed or corroded margins (Fig. 3 a, c, d, e) considered to reflect the late-stage carbonate-rich deuteric or hydrothermal alteration that pervades the central zone of the Walgidee Hills lamproite. The corroded haggertyite is commonly rimmed by irregular-shaped secondary barite (Fig. 3b, d, e). Compositions of the haggertyite and co-existing phases are given in Tables 1 and 2. The whole rock analysis of this samples indicates similar TiO_2, K_2O and Fe contents but lower MgO (~8 wt%) and higher BaO contents (~1.8 wt%) compared to the other haggertyite-bearing lamproites in the intrusion.

Ellendale 9

Haggertyite occurs in the groundmass of a more coarsely crystallized Ti-K-richterite−phlogopite−olivine lamproite from near the centre of the Ellendale 9 pipe together with chromian spinel, perovskite, and rare ilmenite. The spinels range in composition from titanian magnesiochromite and titaniferous chromite with 3−5 wt% TiO_2, 3−7 wt% MgO and 46−56 wt% Cr_2O_3 through titanian chromian magnetite with ~10 wt% TiO_2, 3−5 wt% MgO and 20−30 wt% Cr_2O_3 to titaniferous magnetite (Jaques 2016). The haggertyite occurs as subhedral groundmass grains mostly less than 60 μm (rarely up 100 μm) across (Figs. 2 e, f). Compositions of the haggertyite and co-existing ilmenite are given in Tables 1 and 2. Haggertyite, together with other groundmass phases, has also recently been found as tiny inclusions in olivine phenocrysts in an Ellendale 9 olivine lamproite (A. Abersteiner, personal communication).

HAGGERTYITE COMPOSITION

Average and representative compositions of the haggertyite are given in Table 1 and of the co-existing phases in Table 2. The full data set (~100) of haggertyite analyses by WDS and EDS are given in Supplementary Material.

Major elements

The haggertyite in several of the Walgidee Hills samples (213 and 353) is of similar composition and shows only relatively small differences between grains (Table 1). In addition to Mn and Mg these haggertyites contain minor amounts of V, Cr, Ni and Na, and are very similar in composition to the type haggertyite in xenoliths in the Prairie Creek lamproite (Grey et al. 1998; Velde 2000), apart from being poorer in Cr, Ni and, in most cases, Mg (Table 1). Structural formulae for the haggertyite in samples 213 and 353 closely approximate the ideal haggertyite structure $AM_{12}O_{19}$ with an average composition of $(Ba_{0.7}K_{0.3})_{1.0}[Ti_{5.0}Fe^{3+}_{2.1}Cr_{0.1}Fe^{2+}_{3.8}Mn_{0.2}Mg_{0.6}Na_{0.1}]_{12}O_{19}$ when calculated based on 13 cations and 19 O atoms

(Table 1). Ferrous and ferric iron contents calculated on the basis of charge balance and the ideal $AM_{12}O_{19}$ formula indicates an Fe^{2+}/ Fe^{3+} ratio of ~2:1 (1.8 and 1.6 for samples 353 and 213 respectively), similar to that reported for haggertyite from Prairie Creek (Grey et al. 1998; Velde 2000). The Walgidee Hills haggertyites coexist with priderite with an average composition close to $(K_{1.0}Ba_{0.33})_{1.3}(Ti_{6.7}Fe^{3+}_{1.0}Mg_{0.2})_8O_{16}$ (Table 2).

The haggertyite in Ellendale 9 and Walgidee Hills sample 087 differ from the above haggertyites in having significant variations in Fe and Ti, and in Fe^{3+}/Fe^{2+} (Table 1), and an inverse correlation of Ti and Fe, and Ti and Fe^{3+} (Fig. 4). The Ellendale 9 haggertyites have higher Fe (40–46 wt% Fe as FeO) and lower TiO_2 (37–39 wt%) corresponding to ≤ 5Ti atoms per formula unit (apfu, Table 1; Fig. 4). Ferric iron calculated assuming 13 cations and 19 O atoms are >2 apfu (2.06–2.82). In contrast, the haggertyites in Walgidee Hills sample 087 range to higher TiO_2 (38–43 wt%) and average lower Fe^{3+} contents with ≥5 Ti apfu and ≤2 Fe^{3+} and ≥4 Fe^{2+} apfu (Table 1, Supplementary Material; Fig. 4). Haggertyite in sample 087 shows considerable variation in Cr and, to a lesser extent Mg, within and between grains, with lower Cr associated with higher Ti and lower Fe.

The linear inverse correlation of Ti^{4+} and Fe^{3+} (Fig. 4 b, c) and high correlation of 2 Fe^{3+} with $Ti^{4+} + Fe^{2+}$ (R^2 = 0.908) indicates the dominance of the coupled substitution $Ti^{4+} + Fe^{2+} \leftrightarrows 2\ Fe^{3+}$. The relatively low Cr_2O_3 contents (≤2.4 wt%) in both the Walgidee Hills and Ellendale 9 haggertyites limits the $Ti^{4+} + Fe^{2+} \leftrightarrows 2\ Cr^{3+}$ substitution found by Grey et al. (1998) in the Prairie Creek haggertyite but a weak negative correlation of Ti + Fe with Cr is evident in the Ellendale 9 haggertyite analyses.

Barium is the dominant cation in the A site but the K/Ba ratio in the Ellendale 9 haggertyite is lower (~0.3) than that in the Walgidee Hills haggertyites (~0.4−0.5), which is similar to that in the type haggertyite from the Prairie Creek lamproite.

Trace elements

Trace element analysis by LA-ICP-MS haggertyite in sample 353 shows that the Walgidee Hills haggertyite, in addition to minor amounts of Na, V, Cr, and Ni, also contains small amounts of Si, Ca, Co, Zn, Sr, Zr, Nb, and

Pb, and traces of Al, P, Rb, Hf and Ta (Table 3). Abundances of REE are very low (mostly ≤ 0.1 ppm), lower than found for coexisting priderite (Table 3).

The Walgidee Hills haggertyite coexists with priderites with an average composition $(K_{1.0}Ba_{0.33})_{1.33}(Ti_{6.7}Fe^{3+}_{1.0}Mg_{0.2})_8O_{16}$ (Table 2). The priderite also contains small amounts of V, Cr and Mg. Compared to priderite the haggertyite accommodates significantly more Fe and more Ba whereas the priderite is richer in Ti and K. Mn is strongly partitioned into the haggertyite. The haggertyite is also preferentially enriched in certain lithophile (Na, Ca, V, Sr, Nb, Ba) as well as the siderophile (Mn, Co, Ni) and chalcophile (Zn, Pb) elements compared with the co-existing priderite. The higher K in the priderite is accompanied by higher Rb abundances (Table 3).

PETROGENESIS OF THE HAGGERTYITE

The haggertyite described from the Prairie Creek lamproite, Arkansas is inferred to be of metasomatic origin, formed in a narrow reaction zone between the olivine lamproite host and serpentinized xenoliths as a result of chemical diffusion between the highly contrasting compositions of the xenolith and the ultrapotassic lamproite magma (Grey et al. 1998; Velde 2000). The haggertyite in both the Walgidee Hills and Ellendale 9 lamproites, in contrast, forms part of a magmatic crystallization sequence and crystallizes with other titanates – perovskite, priderite and, commonly, ilmenite as well as K-bearing silicates (titanian phlogopite, titanian potassium richterite), wadeite, and leucite. In the Walgidee Hills lamproite haggertyite appears to be restricted to those lamproites immediately surrounding and immediately within the central zone where it is strongly associated with Ti-K-richterite, a relatively late-forming phase that commonly comprises up to 15 vol% of the host rock. The haggertyite apparently crystallized over a relatively limited temperature interval, forming after priderite (and chrome spinel) and before jeppeite and noonkanbahite in the most evolved rocks at the centre of the lamproite. In the Ellendale 9 lamproite haggertyite has only been found to date in the more coarsely crystallized and evolved K-richterite-bearing phlogopite−olivine lamproites near the centre of the pipe.

The controls on crystallisation of haggertyite are poorly known as experiments to define its stability field are lacking. Crystallization of haggertyite probably reflects and, is a consequence of, the high K, Ti, and Ba contents and relatively Fe-rich state of the lamproite magma at the time of crystallization. However, the bulk composition alone seems unlikely to control haggertyite crystallisation or else haggertyite would be more widespread, in both the Ellendale lamproites and the Walgidee Hills lamproite.

Crystallization temperatures have been estimated from olivine-spinel Mg-Fe exchange between co-existing olivine and chromian spinel for the Ellendale 9 olivine lamproite to range from ~1200 ^{o}C based on titaniferous aluminous magnesiochromite in the early formed tuffs and lavas to ~600 ^{o}C for late-crystallizing titanian chromian magnetite in more extensively crystallized and evolved lavas at the centre of the lava lake (Stachel and Brey 1993; Jaques 2016). The evolved late-crystallizing spinels record a late oxidation event in which fO_2 rose sharply from relatively reducing conditions near the magnetite−wüstite (MW) buffer (MW +1−2 log units) to strongly oxidizing conditions up to 3 log units above the fayalite−magnetite−quartz (FMQ) buffer reaction. The groundmass spinels in sample 79211086 indicate crystallization temperatures of ~790−660 ^{o}C and fO_2 ranging from 1 log unit below to 3.2 log units above the FMQ buffer (Jaques 2016) using the olivine-spinel thermometer and oxygen barometer of Taylor et al. (1998) which corrects for Ti in spinel. The trend of increased substitution of Fe^{3+} in the Ellendale 9 haggertyite, therefore, directly reflects the extended fractional crystallization of olivine and phlogopite and the late oxidation at the centre of the body recorded by the spinels.

Mössbauer spectroscopy studies of priderites from the central zone of Walgidee Hills lamproite have shown that in these priderites the Fe occurs entirely as octahedrally coordinated Fe^{3+} (Pring and Jefferson 1983; McCammon et al. 1999). The Fe in both jeppeite and noonkanbahite is also thought to be entirely as Fe^{3+} with the Fe in noonkanbahite accommodated in the M1 site (Uvarova et al. 2009). However, the trend shown by the haggertyites in the central zone of the Walgidee Hills lamproite is one of increased Fe^{2+} substitution and counter to the oxidation-associated trend in Ellendale 9. The overlap in compositions of the earlier crystallized haggertyites from the main zone (213, 353, 186) with those in the Ellendale 9 lamproite suggests that the initial

trend of the Walgidee Hills haggertyites was towards higher Fe^{3+} but this trend was reversed in the haggertyites of the central zone.

Perovskites in the Walgidee Hills lamproite show trends of increasing Na, Sr, Nb, REE and U, and decreasing Fe towards the centre of the body (Jaques 2016). Experimental evidence suggests that Fe concentration in perovskite increases with fO_2, (Bellis and Canil 2007). The trends of decreasing Fe in perovskite and increasing Fe^{2+} substitution in the haggertyite in the central zone lamproite (087) compared with the haggertyite in the main zone of the Walgidee Hills lamproite suggests either a decrease in fO_2 or perhaps that Fe, and Fe^{3+}, was increasingly sequestered by increased modal abundances of co-existing priderite, ilmenite, and jeppeite. An abundance of late calcite veins throughout the central zone and the immediately surrounding main zone suggests crystallization of the central core of the Walgidee Hills lamproite occurred under increased pCO_2, because of the concentration of volatiles in the residual magma during extended fractionation and slow crystallization.

The low temperatures (850−600 ^{o}C) obtained by olivine-spinel thermometry based on the chromian spinels in the outer margins of the Walgidee Hill lamproite suggest slow cooling and re-equilibration (Jaques 2016). The presence of jeppeite (sample 087) limits the crystallization temperature to ~800 ^{o}C as experiments have shown that above 800 ^{o}C jeppeite breaks down to priderite and other titanate phases (Mitchell and Bergman 1991). Although Fe^{2+} can substitute in priderite, at least at high pressures and under relatively reducing conditions (Foley et al. 1994), the structural formulae of priderite co-existing with haggertyite (Table 2) are comparable with that of the Walgidee Hills priderite found by McCammon et al. (1999) to contain Fe entirely as Fe^{3+}. The similarity of priderite compositions throughout the Walgidee Hills lamproite and the West Kimberley lamproites generally (Jaques 2016) suggests that Fe is also present as Fe^{3+} in these priderites. Olivine-spinel thermobarometry suggests that most of the West Kimberley olivine-bearing lamproites, including those containing groundmass priderite, crystallized under relatively reducing conditions ~MW +1 to 2 log units

(Stachel and Brey 1993; Taylor and Jaques 1998; Jaques 2016). On this basis the prevailing fO_2 late in the crystallization sequence of the Walgidee Hills lamproite could have been close that of the MW buffer.

The identification of magmatic haggertyite in the Walgidee Hills and Ellendale 9 lamproites raises the possibility that haggertyite might also be present, but previously overlooked or perhaps mistaken for ilmenite, in the evolved crystallized groundmass of other olivine lamproites. According to Miller (1996) an unusual K-Ba titanate comparable to the haggertyite found in the Walgidee Hills lamproite was found in the Ellendale 17 olivine lamproite in a separate study. The typically higher Fe contents of olivine lamproites compared to most leucite lamproites in West Kimberley lamproite field suggest that haggertyite is more likely to be found in evolved olivine lamproites than leucite lamproites.

IMPLICATIONS

The discovery of haggertyite ($BaFe_6Ti_5MgO_{19}$) as a magmatic phase in evolved olivine lamproites of the West Kimberley confirms that haggertyite is not an isolated single occurrence but one of an increasing number of minerals in upper mantle rocks and volcanics derived from the upper mantle hosting large-ion-lithophile and high field strength cations. Haggertyite may be present but previously not recognized in other ultrapotassic rocks. It adds to the number of alkali titanate and silicate minerals found in ultrapotassic rocks, notably the lamproites of the West Kimberley region of Western Australia which are the type location for priderite, jeppeite, wadeite, and noonkanbahite. The new data show that haggertyite compositions can vary in their Fe and Ti contents through the coupled substitution $Ti^{4+} + Fe^{2+} \leftrightarrows 2\ Fe^{3+}$ with the Fe^{3+}/Fe^{2+} ratio determined by the prevailing fO_2. Crystallization of haggertyite seems likely to be a consequence of the very high Ba, Ti, and K, and relatively high Fe contents of the evolved lamproite magma and relatively low temperatures.

ACKNOWLEDGEMENTS

The authors acknowledge the facilities and the scientific and technical assistance of Microscopy Australia at the Advanced Imaging Precinct, Australian National University, a facility that is funded by the University, and

State and Federal Governments. We thank Robert Rapp (formerly of RSES, ANU) and Bei Chen (RSES) for assistance with the CAMECA EPMA and LA-ICP-MS analyses respectively, and Antony Burnham and Steve Haggerty as well as Roger Mitchell and the other journal reviewer for constructive comments on the draft manuscript. The project was partially supported by ARC Discovery Project DP140103841.

REFERENCES CITED

Ahmat, A.L. (2012) The Ellendale diamond field: exploration history, discovery, geology and mining. Australian Gemmologist, 24, 280−288.

Bellis, A.J., and Canil, D. (2007) Ferric iron in $CaTiO_3$ perovskite as an oxygen barometer for kimberlitic magmas I: experimental calibration. Journal of Petrology, 48, 219−230.

Ceplecha, J. (2000) 1999 annual report exploration licence 04/832 Walgidee Hills lamproite, Diamond Rose NL. WAMEX Open File Report A59827.

Durey, H. (1998) 1998 annual report exploration licence 04/832 Walgidee Hills, Diamond Rose NL. WAMEX Open File Report A56099 WAMEX Open File Report A59827.

Eggins, S.M., Woodhead, J.D., Kinsley, L.P.J., Mortimer, G.E., Sylvester, P., McCulloch, M.T., Hergt, J.M., and Handler, M.R. (1997) A simple method for the precise determination of >40 trace elements in geological samples by ICPMS using enriched isotope internal standardization. Chemical Geology, 134, 311–326.

Foley, S., Hofer, H., and Brey, G. (1994) High-pressure synthesis of priderite and members of the lindsleyite-mathiasite and hawthorneite-yimengite series. Contributions to Mineralogy and Petrology, 117, 164−174.

Giuliani, A., Phillips, D., Woodhead, J.D., Kamenetsky, V.S., Fiorentini, M.L., Maas, R., Soltys, A., and Armstrong, R.A. (2015) Did diamond-bearing orangeites originate from MARID-veined peridotites in the lithospheric mantle? Nature Communications 6: 1–10 http://doi.org/10.1038/ncomms7837

Grey, I.E., Velde, D., and Criddle, A.J. (1998) Haggertyite, a new magnetoplumbite–type mineral from the Prairie Creek (Arkansas) lamproite. American Mineralogist, 83, 1323–1329.

Haggerty, S.E. (1989) Upper mantle opaque mineral stratigraphy and the genesis of metasomes and alkali-rich melts. In J. Ross et al., Eds., Kimberlites and Related Rocks, Volume 2, Their mantle/crust setting, diamonds and diamond exploration, p. 687−699. Proceedings of the Fourth International Kimberlite Conference, Perth, Australia. Geological Society of Australia Special Publication 14.

Haggerty, S.E. (1995). Upper mantle mineralogy. Journal of Geodynamics, 20, 331–364.

Jaques, A.L. (2016) Major and trace element variations in oxide and titanate minerals in the West Kimberley lamproites, Western Australia. Mineralogy and Petrology, 110, 159–197.

Jaques, A.L. (2017) The Walgidee Hills zoned lamproite intrusion, West Kimberley Province, Western Australia. 11th International Kimberlite Conference Extended Abstract No. 11IKC-4489.

Jaques, A.L., and Foley, S.F. (2018) Insights into the petrogenesis of the West Kimberley lamproites from trace elements in olivine**.** Mineralogy and Petrology, 112, 519–537.

Jaques, A.L., Lewis, J.D., Smith, C.B., Gregory, G.P., Feguson, J., Chappell, B.W., and McCulloch, M.T. (1984a) The diamond-bearing ultrapotassic (lamproitic) rocks of the West Kimberley region, Western Australia. In J. Kornbprobst, Ed., Kimberlites I: Kimberlites and Related Rocks, Elsevier, Amsterdam, pp. 225–254.

Jaques, A.L., Webb, A.W., Fanning, C.M., Black, L.P., Pidgeon, R.T., Ferguson, J., Smith, C.B., and Gregory, G.P. (1984b) The age of the diamond bearing pipes and associated leucite lamproites of the West Kimberley region. Western Australia. BMR Journal of Australian Geoogy and Geophysics, 9, 1–7.

Jaques, A.L., Lewis, J.D., Smith, C.B. (1986) The kimberlites and lamproites of Western Australia. Geological Survey of Western Australia Bulletin 132, 268 pp.

Jaques, A.L., Luguet, A., Smith CB, Pearson, D.G., Yaxley, G.M., and Kobussen, A. (2018) Nature of the mantle beneath the Argyle AK1 lamproite pipe: constraints from mantle xenoliths, diamonds, and lamproite geochemistry. Society of Economic Geologists Special Publication 20, 119–143.

Jarosewich, E., Nelen, J.A., and Norberg, J.A. (1980) Reference samples for electron microprobe analysis. Geostandards Newsletter, 4, 43–47.

Jenner, F.E., O'Neil, and H.St.C. (2012) Major and trace element analysis of basaltic glasses by laser-ablation ICP-MS. Geochemistry Geophysics Geosystems, 13, 1−17, Q03003, doi:10.1029/2011GC003890.

Jochum, K.P., Nohl, L., Herwig, K., Lammel, E., Stoll, B., and Hofmann, A.W. (2005) GeoReM: A new geochemical database for reference materials and isotopic standards. Geostandards and Geoanalytical Research, 29, 333–338.

Jochum, KP., Weis, U., Stoll, B., Kuzmin, D., Yang, Q., Raczek, I., Jacob, D.E., Stracke, A., Birbaum, K., Frick, D.A., Günther, D., and Enzweiller, J. (2011) Determination of reference values for NIST SRM 610–617 glasses following ISO guidelines. Geostandards and Geoanalytical Research, 35, 397–429.

McCammon, C., Mitchell, R.H., and Chakhmouradian, A.R. (1999) Mössbauer spectra of priderite and synthetic iron-bearing hollandite. Canadian Mineralogist, 37, 991–995.

Miller, M. (1996) A mineralogical study of the Walgidee Hills lamproite, West Kimberley Province, Western Australia, 76 p. MSc Thesis, University of Western Australia.

Michell, R.H. (1995) Kimberlites, Orangeites, and Related Rocks, 410 p. Plenum Press, New York.

Mitchell, R.H., and Bergman, S.C. (1991) Petrology of Lamproites, 447 p. Plenum Press, New York.

Norrish, K. (1951) Priderite, a new mineral from the leucite lamproites of the West Kimberley area, Western Australia. Mineralogical Magazine, 29, 496–501.

Paton, C., Hellstrom, J., Bence, P., Woodhead, J., and Hergt, J. (2011) Iolite: Freeware for the visualization and processing of mass spectrometric data. Journal of Analytical Atomic Spectrometry, 26, 2508–2518.

Post, J.E., von Dreele, R.B., and Buseck, P.R. (1982) Symmetry and cation displacements in hollandites: structure refinements of hollandite, cryptomelane and priderite. Acta Crystallography, B38, 1056–1065.

Pouchou, J.L. and Pichoir, F. (1991) Quantitative analysis of homogeneous or stratified microvolumes applying the model "PAP". In K.F.J. Heinrich and D.E. Newbury, Eds., Electron Probe Quantitation, p. 223–249. Plenum Press, New York.

Phillips, D., Clarke, W., and Jaques, A.L. (2012) New $^{40}Ar/^{39}Ar$ ages for the West Kimberley lamproites and implications for Australian plate geodynamics. 12th International Kimberlite Conference, Hyderabad, Abstracts.

Prider, R.T. (1939) Some minerals from the leucite-rich rocks of the West Kimberley area, Western Australia. Mineralogical Magazine, 25, 373–387.

Prider, R.T. (1965) Noonkanbahite, a potassic batisite from the lamproites of western Australia. Mineralogical Magazine, 34, 403–405.

Pring, A., and Jefferson, D.A. (1983) Incommensurate superlattice ordering in priderite. Mineralogical Magazine, 47, 65–68.

Pryce, M.W., Hodge, L.C., and Criddle, A.J. (1984) Jeppeite, a new K-Ba-Fe titanate from Walgidee Hills, Western Australia. Mineralogical Magazine, 48, 263–266.

Stachel, T., and Brey, G. (1993) Spinels in the Ellendale olivine lamproites (Western Australia): significance for diamond distribution and emplacement history. Neues Jahrbuch für Mineralogie – Abhandlungen, 165, 155−167.

Stachel, T., Lorenz, V., Smith, C.B., and Jaques, A.L. (1994) Volcanology and geochemistry of the Ellendale Lamproite Field, (Western Australia). In H.O.A. Meyer and O.H. Leonardos, Eds., Kimberlites, related rocks, and mantle xenoliths, p. 177–194. Companhia de Pesquisa de Recursos Minerais Spec Publ Jan/94, vol 1, Brasilia.

Tappe, S., Pearson, D.G., and Prelevic, D. (2013) Kimberlite, carbonatite, and potassic magmatism as part of the geochemical cycle. Chemical Geology, 419, 1–3.

Taylor, W.R., and Jaques, A.L. (1998) Crystallization history of the Argyle and Ellendale olivine lamproites: constraints from spinel-olivine thermometry and oxygen barometry.7th International Kimberlite Conference, Cape Town, Extended Abstracts.

Taylor, W.R., Kamperman, M., and Hamilton, R. (1998) New thermometer and oxygen fugacity sensor calibrations for ilmenite- and chromian spinel-bearing peridotitic assemblages. 7th International Kimberlite Conference, Cape Town, Extended Abstracts.

Uvarova, Y.A, Sokolova, E., Hawthorne, F.C., Liferovich, R.P., Mitchell, R.H., Pekov, I.V., and Zadov, A.E. (2010) Noonkanbahite, $BaKNaTi_2(Si_4O_{12})O_2$, a new mineral species: description and crystal structure. Mineralogical Magazine, 74, 441–450.

Velde, D. (2000) Mineralogy of mafic xenoliths and their reaction zones in the olivine lamproite from Prairie Creek Arkansas and the paragenesis of haggertyite, $Ba[Fe_6Ti_5Mg]O_{19}$. American Mineralogist, 85, 420–429.

Wade, A., and Prider, R.T. (1940) The leucite-bearing rocks of the West Kimberley area, Western Australia. Quarterly Journal of the Geological Society of London, 96, 39−98.

FIGURE CAPTIONS

Figure 1. Location and geological map of the Walgidee Hills lamproite, West Kimberley region, Western Australia. Points indicate drill hole sample. Numbered samples (087, 213 etc) indicate samples containing haggertyite.

Figure 2. Back-scattered electron (BSE) images of haggertyite. a−b. Images showing subhedral haggertyite (Hag) co-existing with euhedral priderite (Pri) and perovskite (Prv) euhedra in a matrix rich in titanian potassium richterite (KRct) and altered leucite. (c) BSE image showing sub-to euhedral haggertyite grains co-existing with priderite, perovskite and wadeite (Wd) in a matrix with abundant coarse titanian potassium richterite. (d) BSE image showing sub-to euhedral haggertyite grains co-existing with priderite, perovskite and wadeite in a matrix with abundant coarse-grained titanian potassium richterite and minor altered olivine (Ol).

Photographs a-d from Walgidee Hills sample 353. (e) BSE image showing large sub-to euhedral haggertyite grains co-existing with priderite together with euhedral wadeite prisms and perovskite granules in a matrix with abundant coarse titanian potassium richterite and altered former leucite. (f) BSE image showing euhedral haggertyite grains with inclusions of perovskite granules, wadeite prisms and former leucite co-existing with priderite together with euhedral wadeite prisms and perovskite granules in a matrix with abundant coarse-grained titanian potassium richterite and altered former leucite. Photographs e-f from Ellendale 9 sample 79211086.

FIGURE 3. BSE images of haggertyite and associated titanates in the Walgidee Hills lamproite sample 087. (a) Anhedral embayed jeppeite. (b) Subhedral haggertyite rimming euhedral zoned perovskite enclosed in titanian potassium richterite. Note irregularly shaped secondary barite. (c) Subhedral priderite and ilmenite grains with smaller perovskite euhedra in altered matrix. Note secondary barite at margins of priderite grain. (d) Subhedral to haggertyite associated with subhedral to irregularly shaped ilmenite, sub- to euhedral zoned perovskite, and secondary barite. (e) Subhedral haggertyite rimming inclusion of euhedral perovskite. Note secondary barite granules. (f) Small euhedral grain of haggertyite enclosed in potassium richterite. Brt = barite, Hag = haggertyite, Ilm = ilmenite, KRct = potassium richterite, Pri = priderite, Prv = perovskite.

FIGURE 4. Compositional variation in Ti and Fe of haggertyite in the West Kimberley lamproites. (a) Ti versus total iron. (b) Ti versus Fe^{3+}. (c) Inverse linear correlation ($R^2 = 0.908$) of Ti and Fe^{3+} with 2 Fe^{3+} indicating coupled substitution coupled substitution $Ti^{4+} + Fe^{2+} \leftrightarrows 2\ Fe^{3+}$.The trend to higher Fe^{3+} is inferred to reflect increasing fO_2 whereas the trend to higher Fe^{2+} is inferred to indicate reducing fO_2 conditions. Ferric and ferrous iron calculated based on charge balance and 13 cations and 19 O atoms.

TABLES

515 Table 1. Average major element compositions and structural formulae of haggertyite

516 Table 2. Average compositions of co-existing priderite, jeppeite and ilmenite

517 Table 3. Average trace element compositions of haggertyite and priderite

518

519

520

521

Table 1. Average major element compositions and structural formulae of haggertyite

	1			2			3		4	5			6	
	Walgidee Hills									Ellendale 9			Prairie Creek, USA	
	Average	SD	Range	Average	SD	Average	SD	Range		Average	SD	Range	Average	SD
Wt %														
Nb_2O_5	<0.04													
SiO_2	0.06	(0.02)		0.09	(0.01)	0.06			0.09	0.14	(0.07)			
TiO_2	38.72	(0.54)	(38.09−39.90)	38.25	(0.59)	40.69	(1.79)	(38.53−42.50)	42.50	37.91	(0.60)	(36.63−39.16)	39.1	(0.8)
Al_2O_3	<0.03			<0.03		<0.03			<0.03	<0.03				
V_2O_3	0.21	(0.03)	(0.17−0.26)	0.34	(0.02)	0.35	(0.16)	(0.21−0.77)	0.24	0.23	(0.05)	(0.15−0.29)		
Cr_2O_3	0.97	(0.30)	(0.56−1.53)	0.68	(0.31)	0.96	(0.50)	(0.38−2.04)	0.38	0.25	(0.37)	(bld−1.77)	1.4	(1.0)
FeO	40.76	(0.42)	(39.87−41.47)	40.30	(0.22)	39.46	(0.93)	(37.73−41.19)	39.30	43.29	(1.64)	(40.02−46.03)	41.2	(1.0)
MnO	1.27	(0.14)	(1.01−1.46)	0.99	(0.36)	0.77	(0.11)	(0.63−0.88)	0.72	0.82	(0.07)	(0.71−0.93)	0.8	(0.08)
NiO	0.10	(0.03)	(0.06−0.14)	0.09	(0.02)	0.19	(0.18)	(0.03−0.52)	0.25	0.22	(0.11)	(bld−0.42)	0.25	(0.06)
ZnO	0.05	(0.03)		<0.03		0.03			<0.03	0.04				
MgO	2.18	(0.26)	(1.95−2.90)	2.80	(0.23)	1.85	(0.43)	(1.21−2.37)	2.25	2.48	(0.31)	(2.04−3.19)	2.7	(0.5)
CaO	<0.02			<0.02		<0.02			<0.02	0.02				
BaO	10.25	(0.09)	(10.06−10.43)	9.99	(0.14)	10.25	(0.44)	(9.63−10.70)	10.58	11.15	(0.32)	(10.73−11.85)	10.1	(0.2)
Na_2O	0.24	(0.03)	(0.20−0.31)	0.26	(0.03)	0.29	(0.03)	(0.24−0.34)	0.33	0.15	(0.03)	(0.09−0.23)		
K_2O	1.37	(0.03)	(1.31−1.42)	1.47	(0.05)	1.51	(0.03)	(1.47−1.56)	1.50	1.12	(0.11)	(0.90−1.26)	1.42	(0.04)
Total	96.17			95.24		96.40			98.15	97.81			96.97	
Fe_2O_3	15.98			17.11		12.16			11.12	18.76			15.57	
FeO	26.38			24.91		28.51			29.30	26.41			27.19	
Total	97.77			96.96		97.59			99.27	99.69			98.53	
Cations														
Si	0.010			0.015		0.011			0.016	0.023				

This is a preprint, the final version is subject to change, of the American Mineralogist (MSA)
Cite as Authors (Year) Title. American Mineralogist, in press.
DOI: https://doi.org/10.2138/am-2020-7456

Ti	5.057	5.003	5.319	5.447	4.882	5.05
V	0.029	0.047	0.049	0.033	0.032	
Cr	0.133	0.093	0.132	0.052	0.034	0.19
Fe^{3+}	2.088	2.240	1.591	1.426	2.418	2.01
Fe^{2+}	3.832	3.623	4.144	4.175	3.782	3.91
Mn	0.186	0.146	0.113	0.103	0.118	0.12
Ni	0.013	0.012	0.027	0.034	0.031	0.03
Zn	0.006	0.000	0.004	0.000	0.005	
Mg	0.565	0.725	0.478	0.572	0.633	0.69
Ba	0.697	0.681	0.698	0.707	0.748	0.68
Na	0.079	0.089	0.098	0.110	0.050	
K	0.304	0.326	0.334	0.326	0.244	0.31

Analyses 1-4 = Walgidee Hills, 5 = Ellendale 9. 6 = Prairie Creek, USA

1. Average, standard deviation and range of 12 haggertyite analyses, 81210353, Walgidee Hills.
2. Average and standard deviation of 3 haggertyite analyses, 81210213, Walgidee Hills.
3. Average, standard deviation and range of 10 haggertyite analyses, 80210087, Walgidee Hills.
4. Ti-Fe^{2+}-rich haggertyite, 80210087, Walgidee Hills.
5. Average, standard deviation and range of 23 haggertyite analyses, 79211086, Ellendale 9.
6. Average and standard deviation of 56 analyses of haggertyite, Prairie Creek, (Grey et al. 1998).

All analyses by WDS EPMA with Fe determined as FeO and Fe^{3+} and Fe^{2+} calculated assuming 13 cations and 38 O atoms.

522

523

524

Table 2. Average compositions of co-existing priderite, jeppeite and ilmenite

	1		2		3		4		5		6	
			Priderite				Jeppeite		Ilmenite		Ilmenite	
	Mean	1 SD	Mean	1 SD	Mean	1 SD	Mean	1 SD	Mean	1 SD	Mean	1 SD
Wt %												
Nb_2O_5	<0.04											
SiO_2	<0.03		<0.03		<0.03		<0.03		<0.03		0.06	
TiO_2	71.58	(0.64)	72.39	(0.35)	73.65	(0.65)	69.96	(0.59)	54.99	(0.84)	53.41	(0.25)
Al_2O_3	<0.02		<0.02		<0.02		<0.02		<0.02			
V_2O_3	0.13	(0.04)	0.15	(0.04)	0.12	(0.03)	0.18	(0.06)	0.04	(0.02)	0.13	
Cr_2O_3	0.42	(0.18)	0.13	(0.08)	0.16	(0.13)	0.06	(0.05)	0.06	(0.02)	0.19	
Fe_2O_3	11.33	(0.28)	11.47	(0.33)	11.26	(0.45)	4.28	(0.53)	0.38		2.66	
FeO									36.97	(1.80)	35.31	(1.18)
MnO	<0.03		<0.03		<0.03		<0.03		1.91	(0.35)	1.29	(0.06)
NiO	<0.03		0.04		0.04		<0.03		0.04		0.07	
ZnO	<0.03		0.03		<0.03		<0.03		<0.03			

MgO	1.06	(0.23)	0.99	(0.14)	1.00	(0.10)	0.40	(0.07)	5.78	(0.51)	6.35	(1.33)
CaO	<0.02		<0.02		<0.02		<0.02		0.05		0.07	
BaO	7.50	(0.42)	7.30	(0.36)	6.71	(0.39)	15.22	(0.68)				
Na_2O	0.11	(0.02)	0.08	(0.03)	0.11	(0.02)	0.54	(0.04)				
K_2O	6.21	(0.42)	6.28	(0.29)	5.97	(0.40)	8.99	(0.25)				
Total	98.35		98.87		99.01		99.63		100.23		99.53	

Cations	O = 16			O = 13		O = 3	
Si							0.001
Ti	6.637		6.674	6.715	5.517	1.000	0.971
V	0.013		0.015	0.011	0.030	0.000	0.002
Cr	0.041		0.013	0.016	0.010	0.001	0.004
Fe^{3+}	1.051		1.058	1.027	0.338	0.001	0.048
Fe^{2+}						0.748	0.714
Mn						0.039	0.026
Ni						0.001	0.001
Mg	0.195		0.182	0.180	0.063	0.209	0.229
Ca						0.001	0.002
Ba	0.362		0.332	0.319	0.625		
Na	0.053		0.036	0.053	0.221		
K	0.969		0.983	0.924	1.203		
Total	9.321		9.292	9.246	8.006	2.000	2.000

1. Average and standard deviation of 21 co-existing priderite, 81210353, Walgidee Hills.
2. Average and standard deviation of 9 coexisting priderite analyses, 81210213, Walgidee Hills.
3. Average and standard deviation of 22 co-existing priderite analyses, 80210087, Walgidee Hills.
4. Average and standard deviation of 18 co-existing jeppeite analyses, 80210087, Walgidee Hills.
5. Average and standard deviation of 14 co-existing ilmenite analyses, 80210087, Walgidee Hills.
6. Average and standard deviation of 6 co-existing ilmenite analyses, 79211086, Ellendale 9.

All Fe reported as Fe_2O_3 in priderite and jeppeite. Fe determined as FeO and Fe_2O_3 calculated from stoichiometry for ilmenite (2 cations per 3 O atoms).

525

Table 3. Average trace element compositions of haggertyite and priderite

	Haggertyite			Priderite		
	1			2		3
	Average	1 SD	Range	Average	1 SD	

ppm						
Na	1770	202	(1479−1931)	725	44	794
Mg	14363	2611	(12670−18250)	7173	1438	7132
Al	56	18	(37−76)	88	28	65
Si	1628	132	(1530−1810)	1519	230	1400
P	24.6	3.8	(18.9−26.5)	25.6	2.07	19.8
Ca	440	34	(400−482)	46.0	12.3	28.3
Sc	21.6	3.9	(15.9−24.3)	30.1	3.6	31.7
V	1430	125	(1300−1575)	786	211	856
Cr	8451	2211	(5863−11110)	17961	25583	12661
Mn	9854	1120	(8425−10928)	137	39	153
Co	241	14	(230−261)	46.8	8.8	49.6
Ni	863	285	(607−1151)	233	149	142
Cu	1.08	0.09	(0.95−1.15)	2.5	0.08	2.07
Zn	626	51	(578−676)	18.9	0.39	19.3
Ga	0.91	0.23	(0.71−1.18)	0.44	0.11	0.358
Rb	13.7	0.51	(13.2−14.3)	258	9.0	256
Sr	485	47	(145−195)	37.6	15.7	32.0
Y	0.54	0.23	(0.34−0.78)	0.28	0.04	0.809
Zr	167	22	(145−195)	126	43	116
Nb	391	65	(308−462	251	60	278
La	0.49	0.04	(0.46−0.52)	0.635	0.03	0.326
Ce	bld			0.537	0.111	0.427
Pr	bld			0.046	0.006	0.040
Nd	bld			0.120	0.024	0.123
Sm	bld			0.120	0.028	0.055
Gd	bld			0.194	0.027	0.070
Dy	bld			0.015	0.003	0.039
Er	bld			0.008	0.002	0.035
Yb	0.095	(0.012)	(0.081−0.110)	0.012	0.002	0.044
Hf	0.80	0.20	(0.57−1.04)	1.71	0.92	1.82
Ta	0.61	0.39	(0.20−1.12)	7.17	0.99	7.29
Pb	73	6.7	(67−82)	25.3	2.3	24.7
Th	bld			0.025	0.022	0.058
U	0.06	0.03	(0.010−0.077)	0.015	0.002	0.009

1. Average, standard deviation and range of 4 haggertyite analyses, 81210353, Walgidee Hills.

2. Average and standard deviation of 3 priderite analyses, 81210213, Walgidee Hills.

3. Priderite, 81210353, Walgidee Hills (Jaques 2016). bld = below limit of detection.

526

527

528

529

530

531

This is a preprint, the final version is subject to change, of the American Mineralogist (MSA)
Cite as Authors (Year) Title. American Mineralogist, in press.
DOI: https://doi.org/10.2138/am-2020-7456

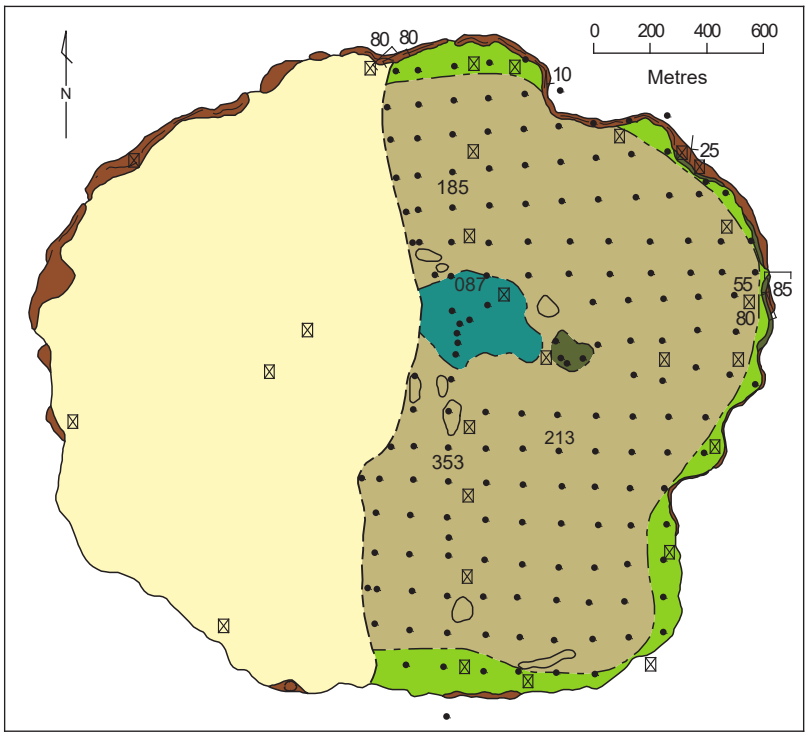

Alluvium, magnesite concretions, calcrete.

WALGIDEE HILLS LAMPROITE

Coarse grained green diopside-K-richterite-sanidine lamproite and lamproite pegmatite.

Medium to coarse grained brown phlogopite-diopside -K-richterite-sanidine lamproite.

Medium grained green olivine-diopside-phlogopite-K-richterite-leucite/sanidine lamproite.

Porphyritic olivine (-leucite) lamproite.

Olivine lamproite crystal tuff (cross sections only).

Olivine lamproite lithic tuff (cross sections only).

Contact breccia and tuff breccia.

BLINA SHALE - TRIASSIC

Grey to brown shale and mudstone, pale brown siltstone and minor sandstone.

Boundary of mapping

25 Strike and dip of bedding.

25 Strike and dip of cleavage.

Pit.

RAB drillhole.

172 RAB drillhole, sample number.

Bulk sample location.

Transitional geological boundary.

This is a preprint, the final version is subject to change, of the American Mineralogist (MSA)
Cite as Authors (Year) Title. American Mineralogist, in press.
DOI: https://doi.org/10.2138/am-2020-7456

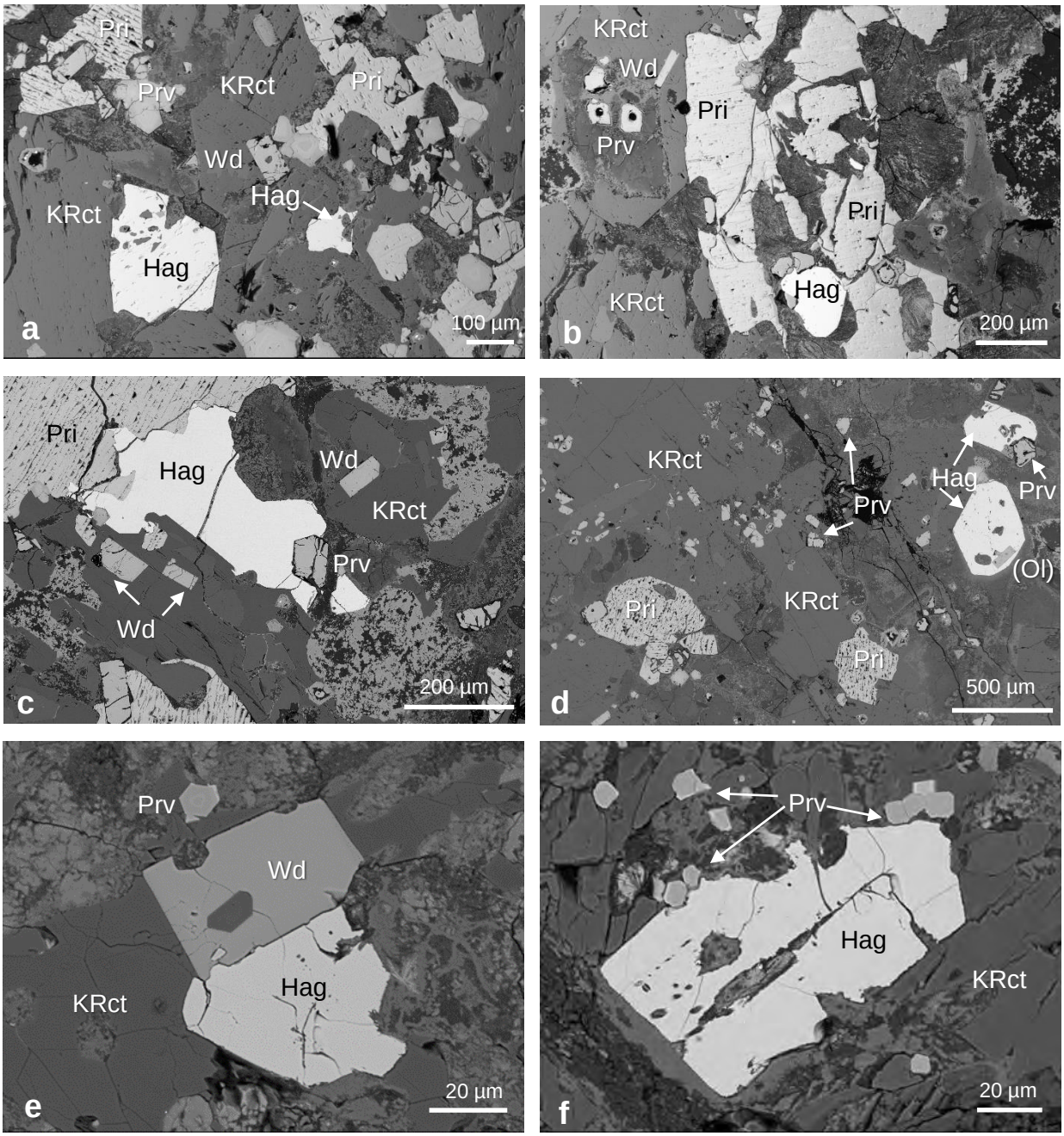

FIGURE 2

This is a preprint, the final version is subject to change, of the American Mineralogist (MSA)
Cite as Authors (Year) Title. American Mineralogist, in press.
DOI: https://doi.org/10.2138/am-2020-7456

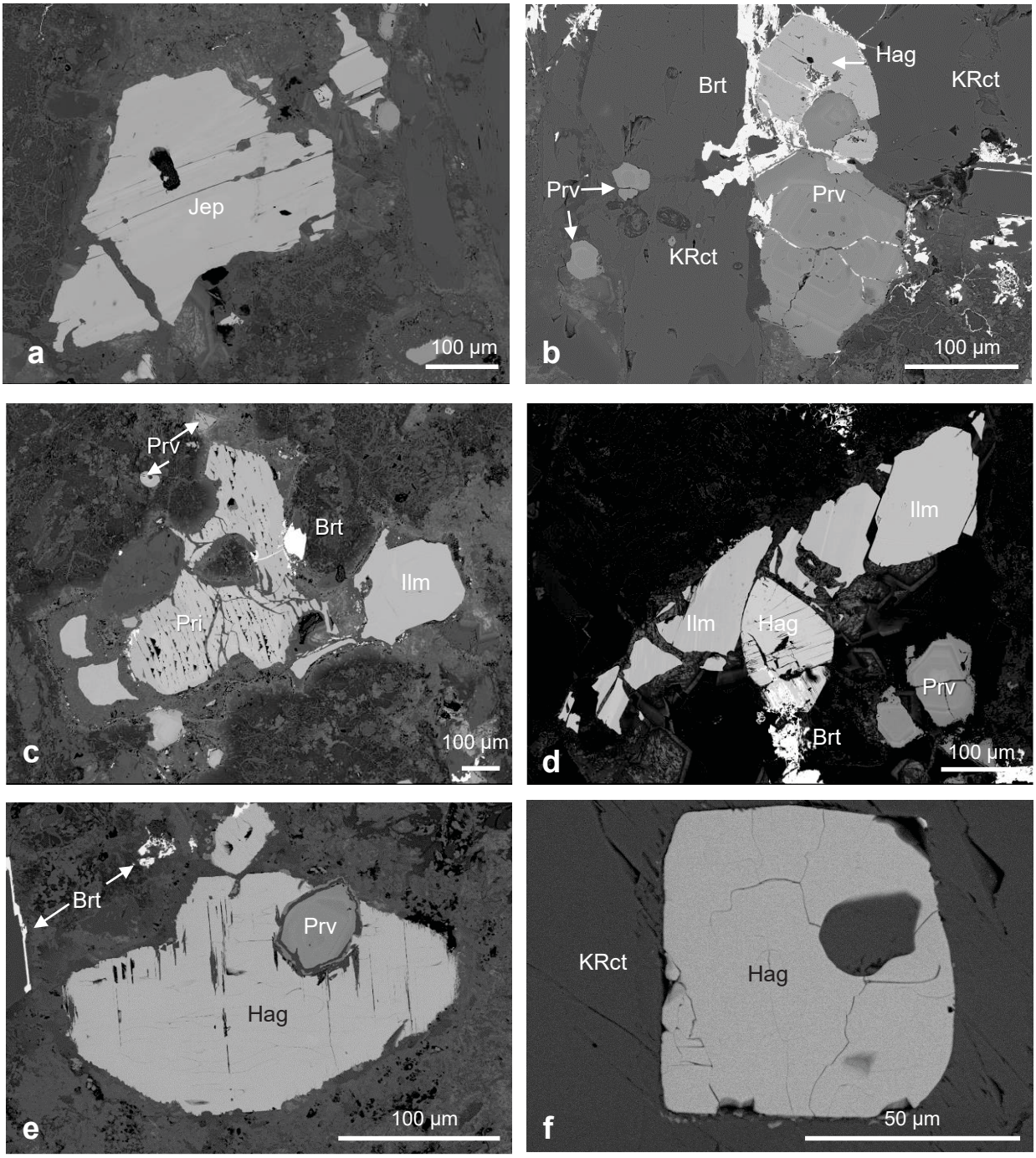

FIGURE 3

This is a preprint, the final version is subject to change, of the American Mineralogist (MSA)
Cite as Authors (Year) Title. American Mineralogist, in press.
DOI: https://doi.org/10.2138/am-2020-7456

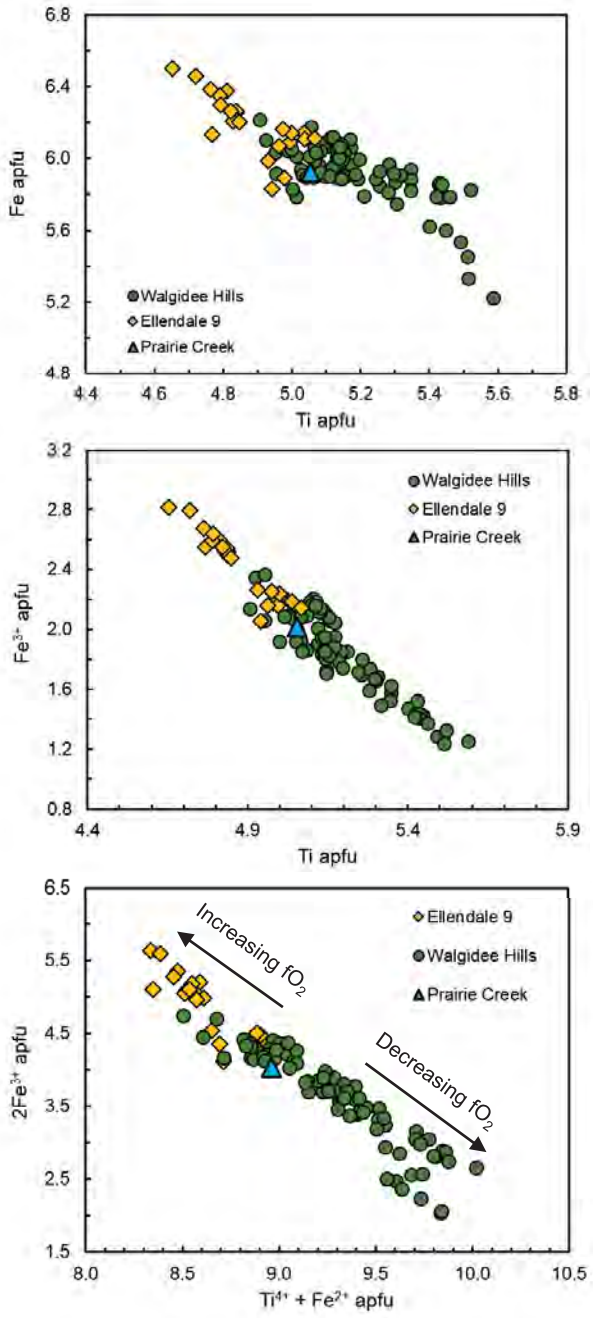

FIGURE 4